Available online at www.sciencedirect.com
ScienceDirect
Trans. Nonferrous Met. Soc. China 34(2024) 3309−3325
Transactions of Nonferrous Metals Society of China
www.tnmsc.cn

3D modeling for effect of tool eccentricity on coupled thermal and material flow characteristics during friction stir welding

Hao SU, Ji CHEN, Chuan-song WU

Key Laboratory for Liquid−Solid Structural Evolution & Processing of Materials, Ministry of Education, Institute for Materials Joining, Shandong University, Jinan 250061, China

Received 4 April 2023; accepted 15 August 2023

Abstract: A novel three-dimensional numerical model is proposed to investigate the effect of tool eccentricity on the coupled thermal and material flow characteristics in friction stir welding (FSW) process. An asymmetrical boundary condition at the tool−workpiece interface, and the dynamic mesh technique are both employed for the consideration of the tool eccentricity during tool rotating. It is found that tool eccentricity induces the periodical variation of the heat densities both at the tool−workpiece interface and inside the shear layer, but the fluctuation amplitudes of the heat density variations are limited. However, it is demonstrated that tool eccentricity results in significant variation of the material flow behavior in one tool rotating period. Moreover, the material velocity variation at the retreating side is particularly important for the formation of the periodic characteristics in FSW. The modeling result is found to be in good agreement with the experimental one.

Key words: friction stir welding; tool eccentricity; thermal behavior; periodic material flow; numerical simulation

1 Introduction

Welding is an important manufacturing technology in industry. Nowadays, many fusion welding methods have been widely applied because of their high efficiency and excellent joining quality, especially for ferrous metal materials [1−3]. In recent years, with increasing demands of lightweight structure and energy conservation, more and more non-ferrous metals like aluminum (Al) and magnesium (Mg) are employed, which can hardly be joined with high-quality due to weld defects like cracks and porosities [4−7]. Therefore, friction stir welding (FSW), as a solid-state joining method with much lower heat input, has been proven to be an appropriate solution for the joining of non-ferrous metals [6−10]. In FSW, a non-consumable tool with high rotational speed is inserted into the workpiece plates, and then moves along the joint line [6,8,9]. Heat is generated by friction at the contact interface between the tool and the workpiece, as well as plastic deformation inside the workpiece material. The heat generation in FSW is highly correlated with both the contact condition at the tool−workpiece interface and the material flow around the tool [4,6−9].

The coupled thermal and mechanical behavior in the FSW process is vitally important for understanding process mechanism, implementing process optimization, as well as promoting process application in production. The periodic material flow and deposition behavior, as well as the onion rings feature, have been indicated as one of the most typical and important phenomena in FSW, and the formation mechanisms have been investigated and discussed continually in the last two decades. KRISHNAN [11] observed in the experiment that

Corresponding author: Hao SU, Tel: +86-15650560065, E-mail: suh@email.sdu.edu.cn
DOI: 10.1016/S1003-6326(24)66610-0

the spacing distance between the periodic markings was equal to the advance distance in one tool rotation period, and proposed that the formation of the periodic behavior or the onion rings was related with the geometric effect of the tool. CHEN et al [12] studied the flow of the shear layer around the tool, and suggested that a portion of shear zone formed a layer which was detached in the trailing−retreating location once in each tool rotating period. CUI et al [13] also found that the spacing of adjacent rings was equal to the distance of tool advance per revolution, and indicated that the horizontal onion ring patterns were resulted from the effect of tool geometry. In addition to the experimental observations, numerical simulation was also employed to visualize the formation of the periodic characteristic during FSW process. For tool with axisymmetric cylindrical/conical pin, the 3D computational fluid dynamics (CFD) based numerical model has been developed and optimized progressively by NANDAN et al [14,15], ARORA et al [16,17], MEHTA et al [18], CHEN et al [19,20], ZHANG et al [21], SU et al [22], ZHAI et al [23], and also many other researchers. Although the model was greatly improved and the coupled thermal−physical behavior of FSW was quantitatively analyzed, the periodic feature has never been presented in the numerical results. Other researchers further considered the effect of tool with non-axisymmetric pins. SU et al [24] proposed a 3D model based on CFD for the tool with three flats on the pin side, and found that the asymmetrical feature of the tool enhanced the material flow velocity and also caused the periodical variations of the process. DIALAMI et al [25] developed a two-stage modeling strategy for the effect of various pin geometries on material flow and welding forces with both slipping and sticking conditions of FSW, and the periodic phenomenon was also obtained. CHEN et al [26] studied the significance of pin thread by proposing a transient CFD model, and found that the material was trapped inside thread groove opening in the high-velocity zone, which caused multiple flow patterns around the threaded pin. HUANG et al [27] established a fluid−solid-interaction algorithm for the coupled modeling of FSW with high depth-to-width ratio tool, which was found to be capable of increasing the strain rate greatly under extremely low heat input, as well as bringing about the periodic dynamic material flow. SUN and WU [28] analyzed the influence of pin thread pitch on the coupled thermal process and material flow in FSW by proposing specific boundary conditions at the tool−workpiece interface, and found that pin thread enlarged the plastic deformation zone and promoted the material mixing.

However, although the abovementioned researches confirmedly identified the important role of asymmetrical tool geometry, many other experimental observations indicated that the periodical characteristics were an extensive characteristic for the tool with symmetrical profile in FSW [29−32]. Moreover, many researchers were gradually conscious of the inevitable tool eccentricity, which was also named as tool oscillation or runout during FSW. YAN et al [33] utilized a linear variable displacement transducer (LVDT) to record tool oscillation along the welding direction, and detected that the measured band spacing in the joint was closely correlated with the oscillation of the welding forces. GRATECAP et al [34] visualized the eccentric movement of FSW tool by utilizing a high-speed camera, and found that the tool eccentricity was the origin of joint surface striations and banded structures. FONDA et al [35] indicated that the onion ring feature in FSW was associated with textural variation along the welding direction, which was proposed to be caused by the oscillation of an off-centered tool. More recently, SU et al [36,37] established a 2D transient model based on CFD to investigate the influence of tool eccentricity in FSW process, and illustrated both the formation and the evolution mechanisms of the periodic material flow behavior in detail. Therefore, more and more evidences made it convinced gradually that the most essential reason for the formation of periodic characteristics in FSW is tool eccentricity, rather than tool geometry. Therefore, it is imperative to have a comprehensive understanding of the periodic thermal physical behavior as a result of tool eccentricity during FSW process.

In this study, a novel 3D transient CFD model is proposed to investigate the effect of tool eccentricity on the coupled thermal and material flow characteristics in FSW. In the model, the specific movement of the rotating tool is taken into consideration, and an asymmetrical boundary condition at the tool−workpiece interface is

employed. Modeling results of heat generation and distribution, temperature distribution, velocity distribution and material flow streamline with and without tool eccentricity during FSW process are quantitatively compared. Particularly, the dynamic evolution for formation of the periodic material flow behavior with tool eccentricity in FSW is demonstrated. For validation of the numerical model, the calculated results of both thermal cycles and material flow distributions around the tool are compared with the measured ones.

2 Experimental

Plates of AA2024-T4 aluminum alloy with length of 200 mm, width of 60 mm and thickness of 6 mm were selected as workpiece material. The tool was made of H13 tool steel, and was composed of a concave shoulder and a conical pin. Besides, the tool was smooth without special feature, the shoulder diameter was 15.0 mm, the pin length was 5.8 mm, and the pin diameter was 4.0 and 6.0 mm at the tip and the root, respectively. The shoulder plunging depth into the workpiece plates was 0.2 mm, and the tilt angle of the tool towards the welding direction was kept at 2.5°. Besides, the welding speed was 80 mm/min, and the tool rotation speed was 800 r/min. Particularly, a foil of AA1060 aluminum with width of 6.0 mm and thickness of 0.2 mm was placed along the welding centerline between the workpiece plates as a marker material to visualize the material flow around the tool during welding. Therefore, a sudden-stop technique was utilized in the experimental procedure, and the tool was pulled out of the workpiece material immediately at the finishing of the welding stage [36]. Several K-type thermocouples were placed inside blind-holes near the tool to record the welding thermal cycles on the workpiece plate during welding [24]. After the welding procedure, the sample was first prepared by cutting the workpiece plate around the exiting keyhole. And then, it was polished in the horizontal cross-section in order to obtain the plane locating 1.4 mm away from the bottom surface of the workpiece plate [36]. Finally, the sample was etched by Keller's reagent to ensure that the marker material distribution around the exiting keyhole was legible, which was then photographed by optical microscopy for the validation with the numerical result.

3 Numerical simulation

The CFD based model for FSW process is normally at steady state for simplification since the coupled thermal mechanical behavior around the axisymmetric tool can be considered to be unchanged after quasi-steady state is achieved. However, it is evident that a steady-state model is not appropriate to study the significance of tool eccentricity. Therefore, a 3D full-coupled transient-state model is proposed. The geometrical details, especially the consideration of tool eccentricity in the model, are schematically displayed in Fig. 1. The computational domain of the model is 6 mm, 120 mm and 200 mm in thickness, width and length, respectively, which is consistent with the sizes of the workpiece plates in the experiment. As can be seen in Fig. 1(a), the center of the shoulder is located at the origin of the coordinate, and the contact interface between the tool and the workpiece material is simplified as specific boundary in the model. The governing equations for the full-coupled 3D transient CFD model of FSW with tool eccentricity can be demonstrated as follows.

Mass conservation equation:

$$\frac{\partial \rho}{\partial t}+\rho\nabla\cdot\vec{V}=0 \tag{1}$$

Momentum conservation equation:

$$\rho\left[\frac{\partial \vec{V}}{\partial t}+(\vec{V}\cdot\nabla)\vec{V}\right]=-\nabla P+\mu\nabla^2\vec{V} \tag{2}$$

Energy conservation equation:

$$\rho c_p\left(\frac{\partial T}{\partial t}+\vec{V}\cdot\nabla T\right)=\nabla\cdot\left(\lambda\nabla T\right)+\Phi \tag{3}$$

where ρ is the density, t is the time, $\vec{V}$ is the velocity vector, P is the pressure, μ is the viscosity, c_p is the specific heat capacity, T is the temperature, λ is the thermal conductivity, and Φ is the volumetric heat source.

As shown in Fig. 1(b), an interior surface around the tool region with a diameter of 20 mm is utilized, which is fixed to ensure the mesh quality around the tool because of tool eccentricity. The dynamic mesh moving technique is employed inside the interior surface, while the mesh remains invariable outside the interior surface. In this model,

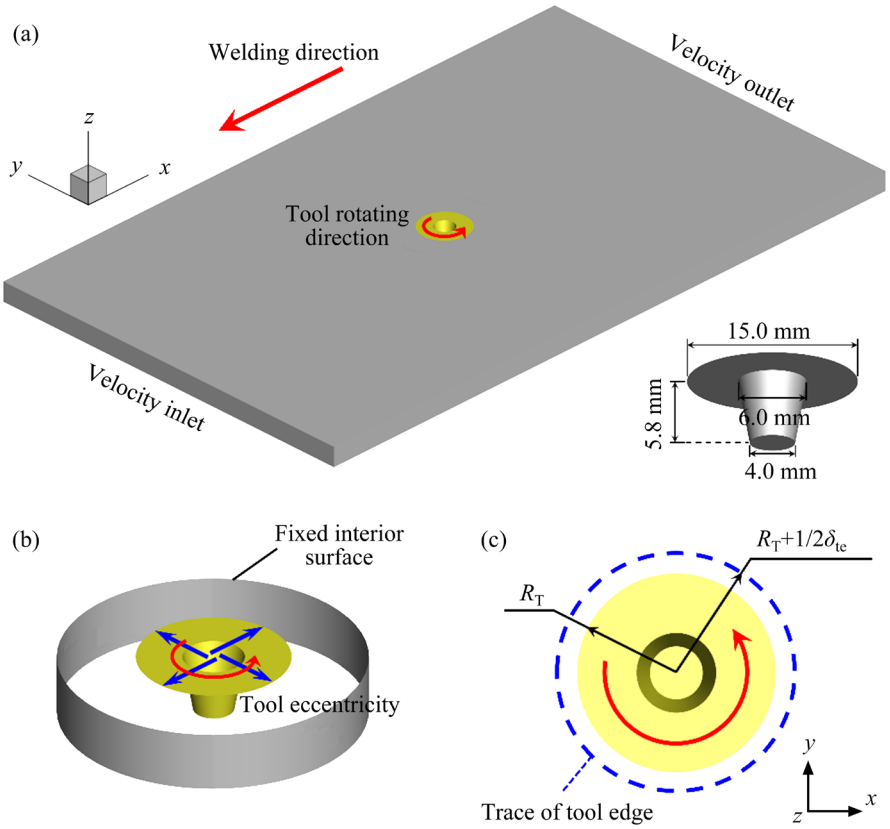

Fig. 1 Schematic diagrams of 3D geometrical model and tool (a), correlation between tool eccentricity and fixed interior surface in 3D model (b), and trace of tool edge with tool eccentricity during FSW (c)

it is assumed that the trace of the rotating tool because of tool eccentricity is a circle. As shown in Fig. 1(c), the maximum radius of the tool/pin edge (R_{trace}) is given by [37]

$$R_{trace}=R_{t/p}+\frac{1}{2}\delta_{te} \tag{4}$$

where $R_{t/p}$ is the radius of the tool/pin, and δ_{te} (=0.06 mm) is the magnitude of tool eccentricity based on experimental measurements [33,34].

The tool movement velocity in x and y direction, i.e., v_{t/p_x} and v_{t/p_y}, respectively, as a result of tool eccentricity can be written as

$$v_{t/p\_x}=\frac{1}{2}\delta_{te}\omega\cos[\omega(t_w-t_0)+\pi] \tag{5}$$

$$v_{t/p\_y}=\frac{1}{2}\delta_{te}\omega\sin[\omega(t_w-t_0)+\pi] \tag{6}$$

where ω is the tool rotational speed; t_w and t_0 are the welding time and the starting time of tool eccentricity, respectively. In the present model, the tool is static before the time t_0=25.00 s to reach a quasi-steady state of thermal−mechanical behavior around the tool.

In FSW, four regions have been defined at the horizontal pin around the tool, which is advancing side (AS), retreating side (RS), leading edge (LE), and trailing edge (TE), respectively. Thus, four quadrants can be divided accordingly as LE/AS, LE/RS, TE/RS, and TE/AS, as schematically shown in Fig. 2. Besides, since the tool eccentricity leads to the dynamic variation of the tool/pin position during tool rotating, it is assigned in this work that one tool rotating period is uniformly divided into eight pin orientations. According to the complicated thermal−mechanical characteristics at the tool−workpiece interface because of tool eccentricity in FSW, it is still intractable to propose a credible methodology of boundary conditions. Therefore, a conventional and well-validated boundary condition is employed, which is based on the relative velocity between the tool and the workpiece material, and a variable δ is utilized to describe the slip rate between the tool velocity v_t(=$r\omega$) and the workpiece material velocity v_m at the contact interface.

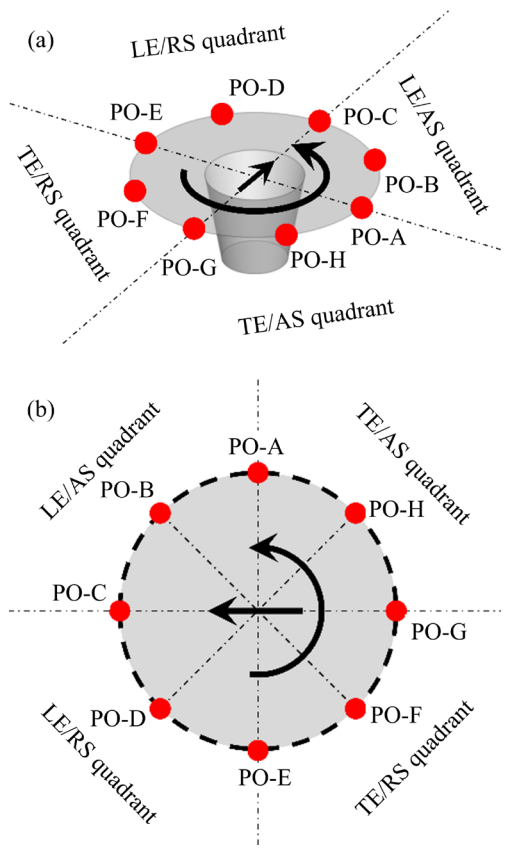

Fig. 2 Schematic diagrams of four quadrants and eight pin orientations during FSW with tool eccentricity: (a) 3D view; (b) 2D view

At the shoulder and the pin bottom, the material velocity is written as [14,22]

$$\vec{v}_{\mathrm{m}}=\delta\vec{v}_{\mathrm{t}} \tag{7}$$

At the pin side, a novel asymmetrical boundary condition is employed according to the experimental observation by GRATECAP et al [34] and the assumptions that have been proposed by SU et al [36].

First, in LE/AS and LE/RS quadrants ($0.5\pi\leq\alpha<1.5\pi$), the softened material is pushed by the rotating tool and is accumulated from LE/AS to LE/RS, and thus, the material velocity can be given by

$$\vec{v}_{\mathrm{m}}=\frac{1}{2}\bar{\delta}\vec{v}_{\mathrm{t}}\left[\cos(\alpha-1.5\pi)+1\right] \tag{8}$$

Second, in TE/RS quadrant ($1.5\pi\leq\alpha<2.0\pi$), it is no doubt that the material starts to be deposited gradually and loosens the engagement with the rotating tool, so the material velocity can be given by

$$\vec{v}_{\mathrm{m}}=\frac{1}{2}\bar{\delta}\vec{v}_{\mathrm{t}}\left[\cos(2\alpha-3.0\pi)+1\right] \tag{9}$$

Moreover, in TE/AS quadrant ($2.0\pi\leq\alpha<2.5\pi$), it is assumed that there is no contact force according to some experimental observations, so the material velocity is given by

$$\vec{v}_{\mathrm{m}}=0 \tag{10}$$

where $\bar{\delta}$ is the average value of the slip rate between the tool and the workpiece material, and α is the angle between the normal direction of tool velocity v_{t} and x-axis.

Both the volumetric heat source inside the shear layer around the rotating tool and the frictional heat flux at the tool−workpiece interface are considered.

The source term Φ in the energy conservation equation can be expressed as

$$\Phi=\beta_1\sigma\varepsilon \tag{11}$$

where β_1 is the thermal conversion efficiency of plastic deformation, σ is the flow stress, and ε is the effective strain rate.

Besides, the frictional heat flux is given as follows.

At the shoulder and the pin bottom, the heat flux can be expressed as

$$q_{\mathrm{o}}=\beta_2\left[\bar{\delta}\tau_{\mathrm{y}}+(1-\bar{\delta})\mu_{\mathrm{f}}p_0\right]r\omega \tag{12}$$

At the pin side, the heat flux can be expressed as

$$q_{\mathrm{o}}=\beta_2\left[\bar{\delta}\tau_{\mathrm{y}}+(1-\bar{\delta})\mu_{\mathrm{f}}p_0\sin\xi\right]r\omega \tag{13}$$

where β_2 is the thermal conversion efficiency of frictional heat, τ_{y} is the shear yield stress, μ_{f} is the friction coefficient, p_0 is the pressure of the tool, and ξ is the taper angle of the pin.

A variable φ is utilized to define the percentage of heat transferred into the workpiece material, which is correlated with the density, the thermal conductivity and the heat capacity of both the tool and the workpiece material, and is estimated by [14]

$$\varphi=\frac{\sqrt{(\rho\lambda c_p)_{\mathrm{W}}}}{\sqrt{(\rho\lambda c_p)_{\mathrm{W}}}+\sqrt{(\rho\lambda c_p)_{\mathrm{T}}}} \tag{14}$$

where the subscripts “W” and “T” represent the workpiece and the tool, respectively.

The boundary condition for heat exchange at

different surfaces of the workpiece material is given as follows.

At the top surface, both the heat transfers by radiation and convection should be considered, which can be written as

$$-\lambda\frac{\partial T}{\partial z}\bigg|_{\text{top}}=\sigma_{\text{b}}\varepsilon_{\text{b}}(T^4-T_{\text{a}}^4)+h_{\text{t}}(T-T_{\text{a}}) \tag{15}$$

At the bottom surface, the heat is transferred into the backing plate, which can be written as

$$\lambda\frac{\partial T}{\partial z}\bigg|_{\text{bottom}}=h_{\text{b}}\,(T-T_{\text{a}}\,) \tag{16}$$

where σ_{b} is the Stefan−Boltzmann constant, ε_{b} is the emissivity, T_{a} is the ambient temperature, and h_{t} and h_{b} are the coefficients of heat transfer at the top and the bottom surface, respectively.

The material properties and other parameters in the above-mentioned equations are consistent with the data that have been published in the literature [22,24].

4 Results and discussion

4.1 Thermal behavior

It is evident that the heat generation due to both interfacial friction and plastic deformation during FSW without tool eccentricity has been widely investigated in the literature, and no periodic phenomenon has been reported [14−23]. However, the heat generation changes continually with tool eccentricity, as can be observed in Fig. 3. First, for the frictional heat at the tool−workpiece interface, it can be seen from Fig. 3(a) that the heat generation rate at the shoulder is much higher than that at the pin, and both values demonstrate periodical features during tool rotating. It is clearly shown that the variation amplitude of heat generation is no more than 1 W, which can be neglected compared with the total value of about 1109 W at the shoulder. In addition, the total heat generated at the pin is in the range of 70−74 W, and the more evident periodical feature should be caused by the continuous changing of both the interfacial contact condition and the relative material flow velocity between the pin and the workpiece material. It is shown that the heat generated at the pin increases gradually from PO-A, achieves the maximum value at PO-D, and then decreases persistently until it reaches the minimum value at PO-H. Second, for volumetric heat generated by plastic deformation in the stirring zone, the variation of the integrated heat generation shows a periodic feature with sinusoidal function approximatively, as can be seen in Fig. 3(b). It is found that the maximum value is about 543 W, which is achieved at PO-D, while the minimum value is about 535 W, which is achieved between PO-G and PO-H. Moreover, it can be calculated that the variation amplitude of heat generation is only 12 W, which is less than 0.7% of the total value, i.e., 1720 W during one tool rotating period in FSW with tool eccentricity.

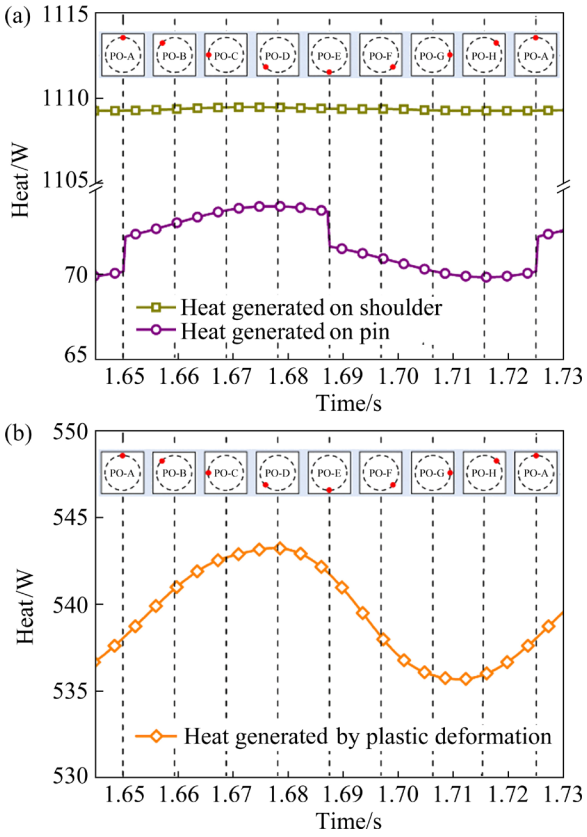

Fig. 3 Heat generation during FSW with tool eccentricity: (a) Heat generated by friction at tool−workpiece interface; (b) Heat generated by plastic deformation in stirring zone

To have a better understanding of the frictional heat generation variation on the pin, Figs. 4 and 5 are displayed to compare the heat flux distribution at the interface during FSW process without and with tool eccentricity. As the asymmetrical boundary condition is employed in the model, the heat flux density is relatively higher at the LE than that at the TE. Besides, the heat flux density is also higher at the RS than that at the AS, which is caused by the higher material flow velocity in the

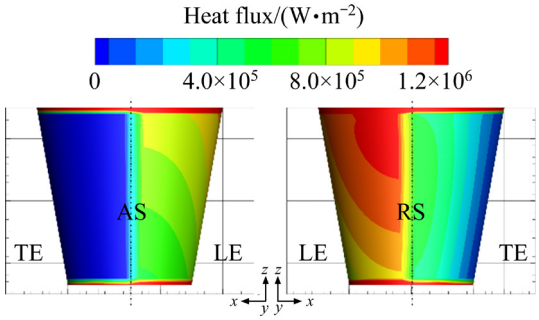

Fig. 4 Heat flux distribution at interface between pin side and workpiece material during FSW without tool eccentricity

corresponding region. Therefore, the maximum heat flux density reaches over 1.2×10^6 W/m^2 and is found to be located in the LE/RS quadrant, while the minimum heat flux density is 0 because there is no substantial contact between the tool pin and the workpiece material in the TE/AS quadrant [36]. It can be seen that the distribution pattern of the heat flux density on the pin reveals insignificant difference for various pin orientations with tool eccentricity, and is also found to be similar with that without tool eccentricity during FSW. For more details, it is shown in Fig. 5 that high magnitude region of the heat flux density varies in the LE/RS quadrant at different pin orientations, and the maximum and the minimum values appear at PO-D and PO-H, respectively, which is consistent with the variation tendency of the heat generation rate.

Figures 6 and 7 demonstrate the volumetric heat density distribution inside the shear layer during FSW without and with tool eccentricity, respectively. It is shown that the maximum value of volumetric heat density exceeds 1.0×10^{10} W/m^3, which is found to be located at the edge of shoulder for the condition without tool eccentricity, as well as for various pin orientations with the tool

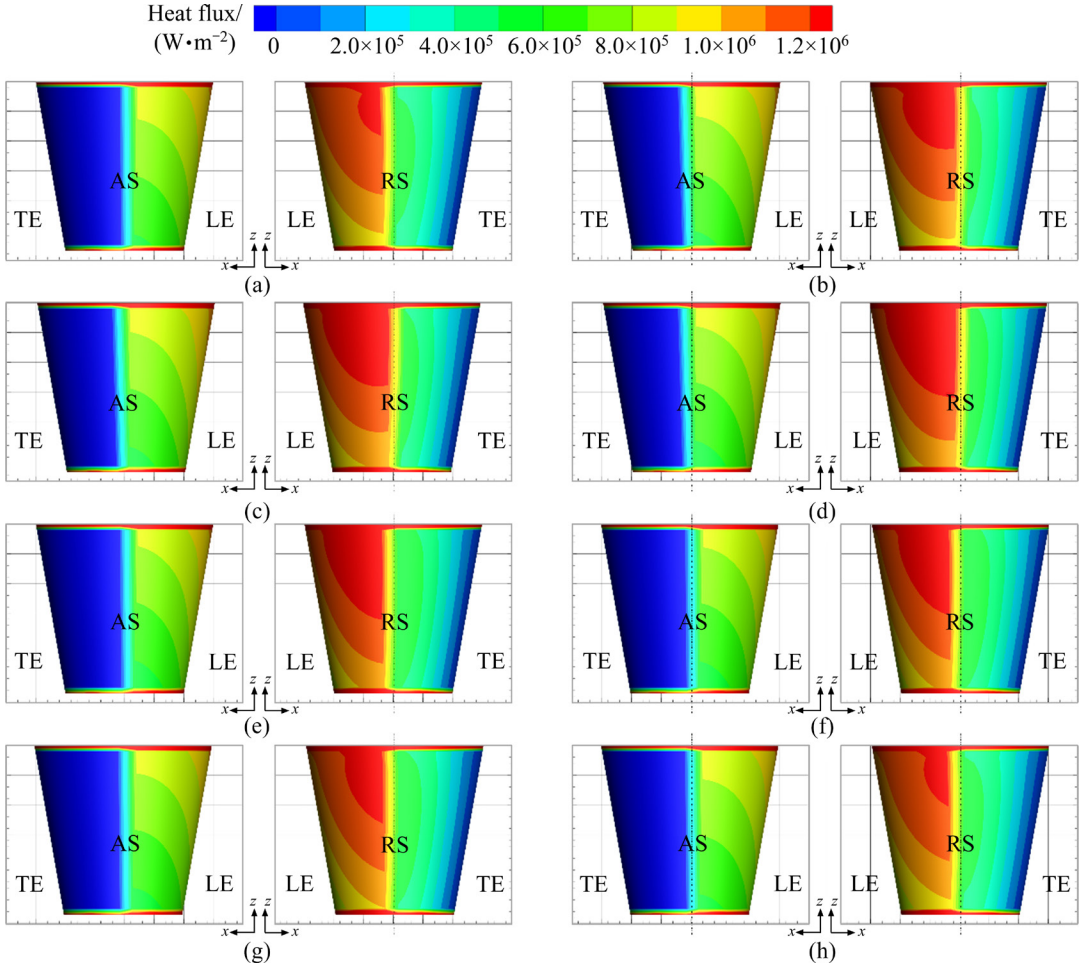

Fig. 5 Evolution of heat flux distribution at interface between pin side and workpiece material during FSW with tool eccentricity at various pin orientations: (a) PO-A; (b) PO-B; (c) PO-C; (d) PO-D; (e) PO-E; (f) PO-F; (g) PO-G; (h) PO-H

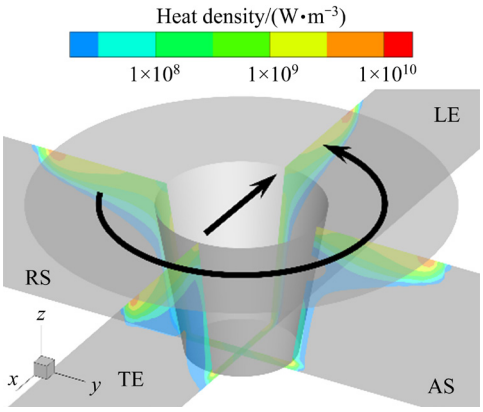

Fig. 6 Volumetric heat density distribution inside shear layer during FSW without tool eccentricity

eccentricity. In FSW, the volumetric heat is generated by plastic deformation, and has positive correlations with both the material flow velocity and the material viscosity inside the shear layer [15,19,24]. As a result, the volumetric heat density is higher at the RS than that at the AS, and is also higher at the TE than that at the LE during welding without tool eccentricity, as shown in Fig. 6. It is no doubt that tool eccentricity would lead to the variations of material flow velocity, strain rate and also material flow stress according to the Sellars−Tegart constitutive law [14,38]. Therefore, the distribution of volumetric heat density changes continuously near the rotating tool during welding

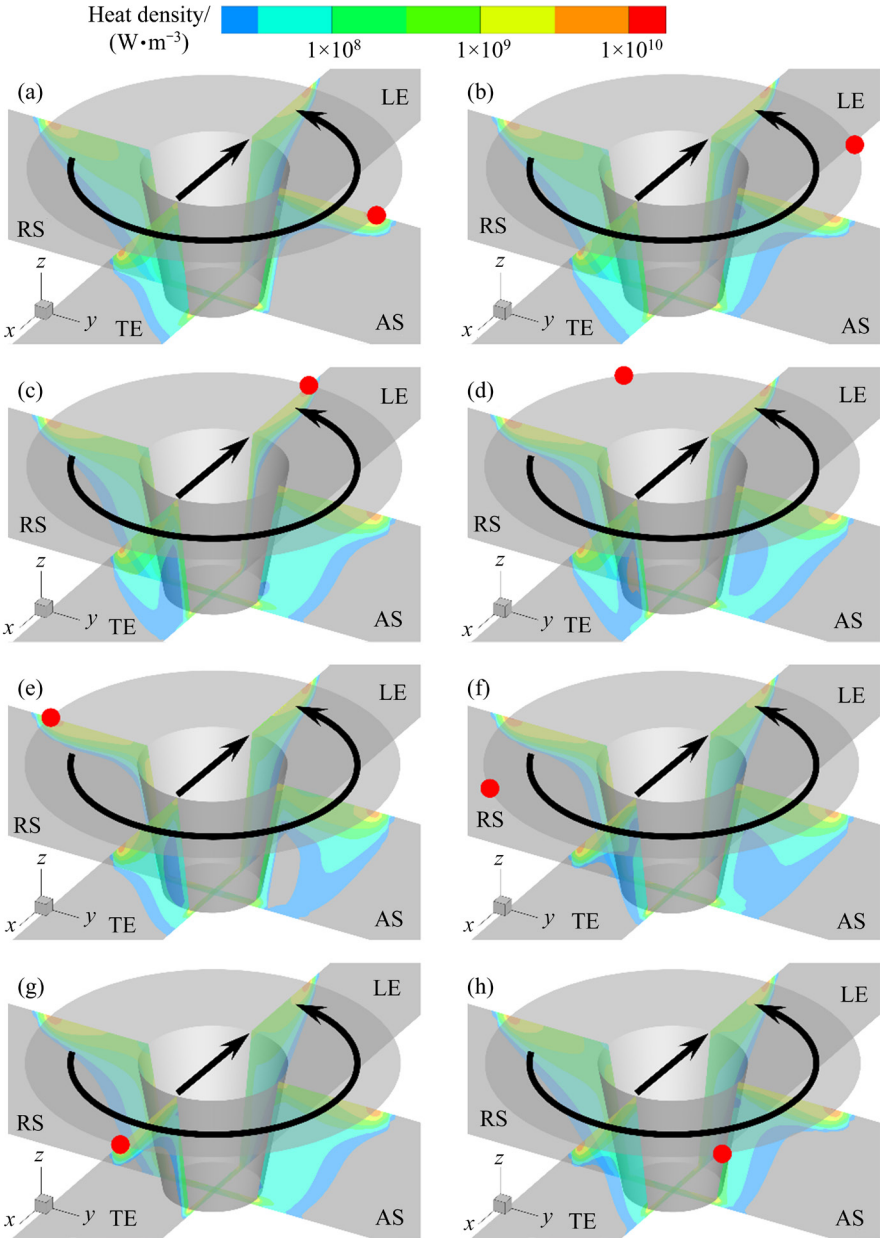

Fig. 7 Evolution of volumetric heat density distribution inside shear layer during FSW with tool eccentricity at various pin orientations: (a) PO-A; (b) PO-B; (c) PO-C; (d) PO-D; (e) PO-E; (f) PO-F; (g) PO-G; (h) PO-H

with tool eccentricity, as can be seen in Fig. 7. It is found that the volumetric heat density is relatively lower at AS, LE, RS and TE than that at other regions as the tool eccentricity moves to the corresponding position with the pin orientation of PO-A (Fig. 7(a)), PO-C (Fig. 7(c)), PO-E (Fig. 7(e)) and PO-G (Fig. 7(g)), respectively. Besides, it is also shown that the volumetric heat density is lower at LE/AS, LE/RS, TE/RS and TE/AS than that at TE/RS, TE/AS, LE/AS and LE/RS with the pin orientation of PO-B (Fig. 7(b)), PO-D (Fig. 7(d)), PO-F (Fig. 7(f)) and PO-H (Fig. 7(h)), respectively. By comparative analysis between Figs. 6 and 7, it is believed that the main reason for the variation of volumetric heat density is the transformation of the material flow velocity around the tool at different pin orientations, which changes both the material stress and the material viscosity with tool eccentricity.

According to the above-mentioned analysis, it is demonstrated clearly that both the frictional and the volumetric heat density distributions during FSW are influenced by tool eccentricity at different pin orientations. However, the variation of the total heat generation is found to be insignificant for both welding conditions with and without tool eccentricity. Therefore, the temperature distribution at the pin is found to be similar approximately whether there is tool eccentricity or not during FSW, as comparatively shown in Figs. 8 and 9. It can be seen that the temperature at the TE is higher than that at the LE, and the maximum temperature at the pin, which reaches over 790 K, is located between TE/AS and TE/RS quadrants near the shoulder. Besides, there is a region with temperature below 730 K located between LE/AS and LE/RS quadrant at the lower part of the pin. Another important phenomenon is that the tool eccentricity doesn't lead to evident difference of temperature distribution around the pin at various pin orientations during the tool rotating, as can be observed in Fig. 9. Consequently, it is no doubt that the effect of tool eccentricity on the temperature distribution and evolution inside the workpiece material is also insignificant during tool rotating. Figure 10 compares thermal cycles between calculated and measured results of two points at 10 and 20 mm away from the welding centerline at the AS. It is shown that there is no evident difference between the calculated thermal cycles with and without tool eccentricity, and both the calculated results are in good agreement with the measured ones.

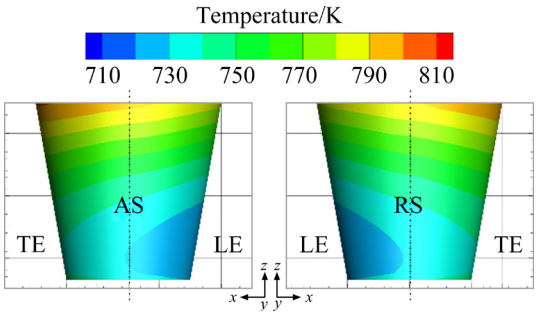

Fig. 8 Temperature distribution at interface between pin side and workpiece material during FSW without tool eccentricity

4.2 Plastic material flow

Figure 11 presents the material flow velocity magnitude and direction around the pin at z=−4.5 mm horizontal plane during FSW without tool eccentricity. It can be seen in the velocity magnitude distribution that the material flow velocity at the LE and the RS is higher than that at the TE and the AS, respectively, which is considered as a result of the asymmetrical boundary condition employed in the model. Since it is known that the material at the front of the pin flows through the RS and finally deposits at the back of the pin, only the material flow directions in the LE/AS and TE/RS quadrants are shown. It can be seen that the gradient of the material flow velocity increases as the material approaches the pin gradually, and as a result, the material flow direction changes rapidly towards the LE/RS quadrant at L-1. Then, both the magnitude and the gradient of the material flow velocity further increase at L-2. And then, the material flow velocity reaches the maximum at L-3 and decreases at L-4, which is located in the TE/RS quadrant. Finally, it is shown that the material flow velocity decreases increasingly at the back of the pin, as the material is deposited gradually at L-5.

Figure 12 demonstrates the evolution of the material flow velocity magnitude around the pin at z=−4.5 mm horizontal plane during FSW with tool eccentricity. In contrast to the results shown in Fig. 11, it is evident that the material flow region changes continuously at different pin orientations, and all of the flow areas around the pin with tool

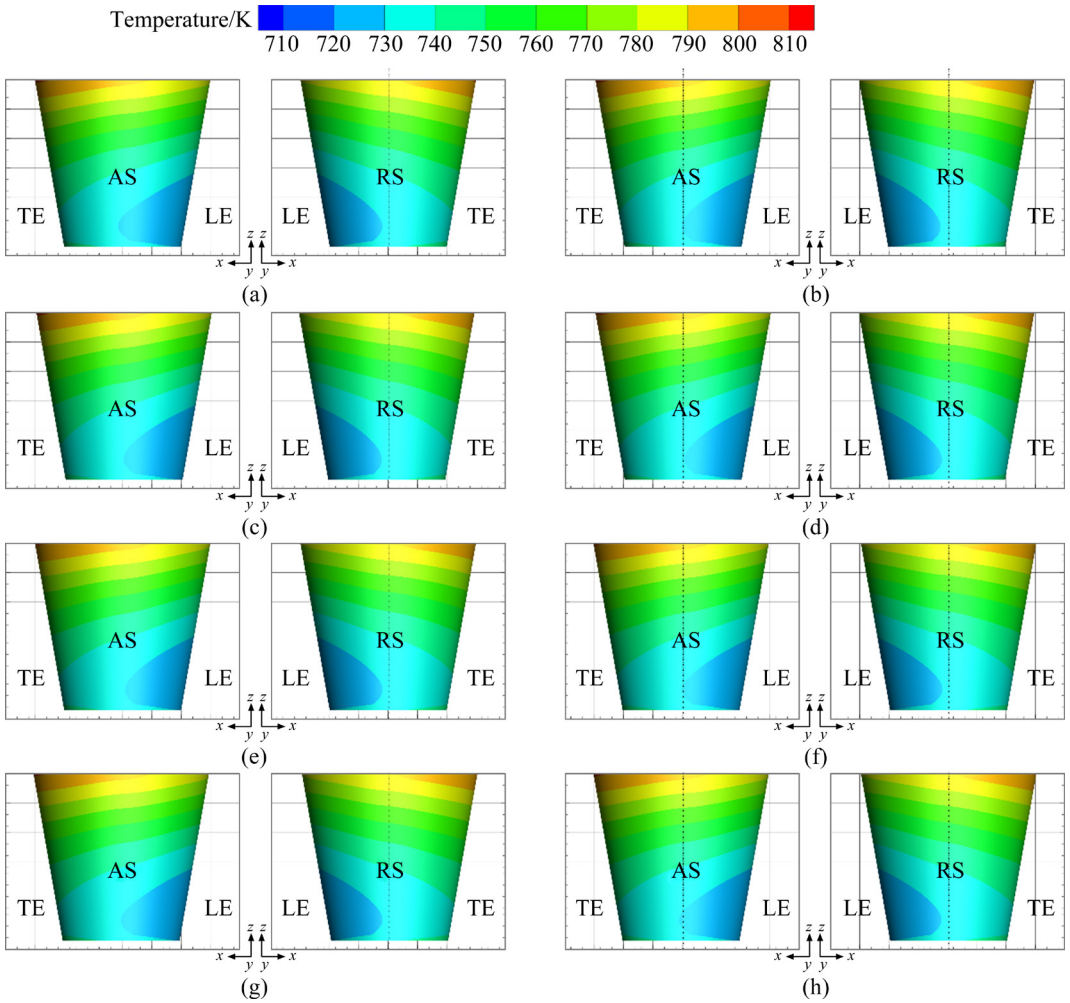

Fig. 9 Evolution of temperature distribution at interface between pin side and workpiece material during FSW with tool eccentricity at various pin orientations: (a) PO-A; (b) PO-B; (c) PO-C; (d) PO-D; (e) PO-E; (f) PO-F; (g) PO-G; (h) PO-H

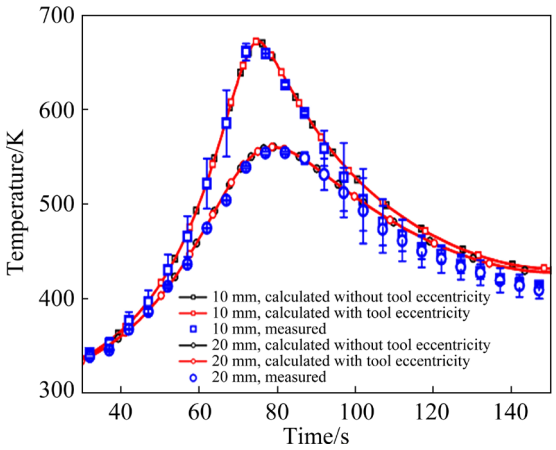

Fig. 10 Comparison of thermal cycles between calculated and measured results

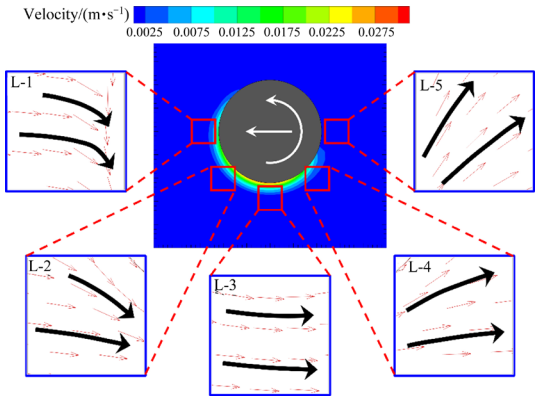

Fig. 11 Material flow velocity magnitude and direction around pin at z=−4.5 mm horizontal plane during FSW without tool eccentricity

eccentricity are also relatively larger than those without tool eccentricity. At PO-A, higher velocity gradient is found to be located at the AS, which corresponds to the position of the pin orientation, as can be seen in Fig. 12(a). With the tool rotating and deviating from the tool center axis as a result of tool eccentricity, it is observed that the relatively high velocity gradient region moves synchronously as

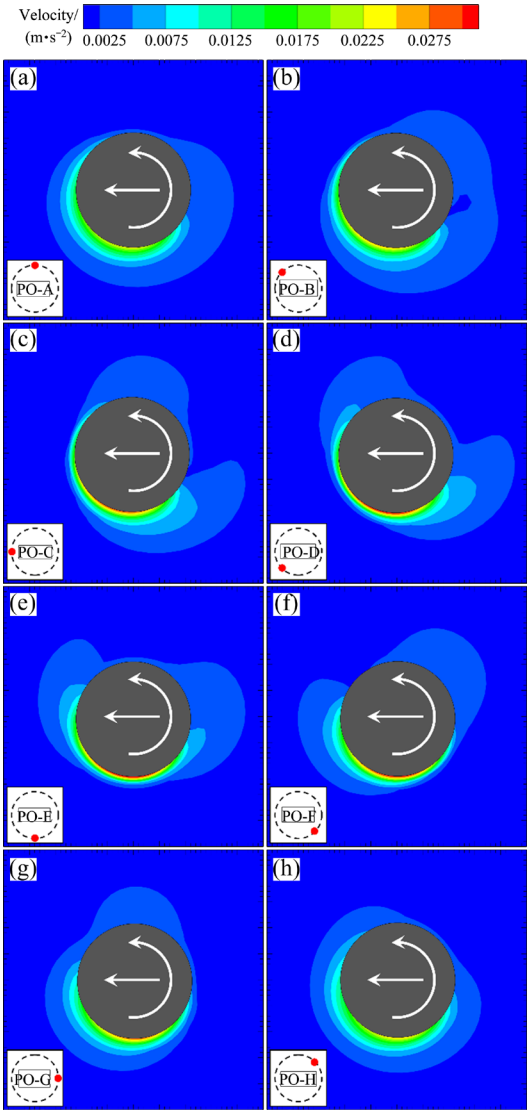

Fig. 12 Evolution of material flow velocity magnitude at z=−4.5 mm horizontal plane during FSW with tool eccentricity at various pin orientations: (a) PO-A; (b) PO-B; (c) PO-C; (d) PO-D; (e) PO-E; (f) PO-F; (g) PO-G; (h) PO-H

the pin orientation changes from PO-A to PO-H. Particularly, the velocity gradient around the pin reaches the maximum value at the RS with the pin orientation of PO-E, as shown in Fig. 12(e). Therefore, it can be deduced that tool eccentricity causes squeezing action on the material around the pin during tool rotating.

Figure 13 further shows the evolution of the material flow direction around the pin at z=−4.5 mm horizontal plane during FSW with tool eccentricity. It looks seemingly that the material flow direction changes continually and also intensely during tool rotating at different pin orientations. At L-1, the material flow direction varies distinctly in a corresponding pattern with the gradient changing of the material flow velocity. However, the basic material flow tendency is consistent since the material flow direction is always towards the LE/RS quadrant at different pin orientations. At L-2, since the material flow velocity increases gradually along the tool rotating direction, the variation amplitude of the material flow direction decreases accordingly. At L-3, it can be seen that the variation of the material flow direction for different pin orientations is relatively lower than that at any other locations, because of the extremely high material flow velocity in this region. At L-4, the material flow velocity decreases gradually, so the variation amplitude of the material flow direction increases. At L-5, as the material flow velocity decreases significantly at the back of the pin, the influence of tool eccentricity on the material flow direction becomes more drastic during tool rotating. In this region, it can be observed that the flow direction with tool eccentricity is similar to that without tool eccentricity at the pin orientations of PO-D, PO-E, PO-F and PO-G, which is along the opposite direction of the tool movement. However, the backward flow direction is also evident with tool eccentricity at the pin orientations of PO-H, PO-A, PO-B and PO-C. As a result, the material is periodically deposited at the back of the pin.

By comparing Fig. 11 with Figs. 12 and 13, it can be known that the influence of tool eccentricity on material flow is significant during FSW. First, the material at the front of the pin flows into the LE/RS quadrant, and its flow velocity increases with the increase of the velocity gradient. However, although both the velocity magnitude and the flow direction change at different pin orientations with tool eccentricity, it is believed that the periodic feature is not primordially formed in this region since the material can pass through this quadrant instantly. Second, the material is deposited gradually in the TE/RS quadrant, its flow velocity decreases more drastically, and the variations of both the velocity magnitude and the flow direction are more evident than those in the LE/RS quadrant. Therefore, the periodic feature starts to form in this region with decreasing the material flow velocity and increasing the variation of the material flow direction. Finally, it is considered that the periodic

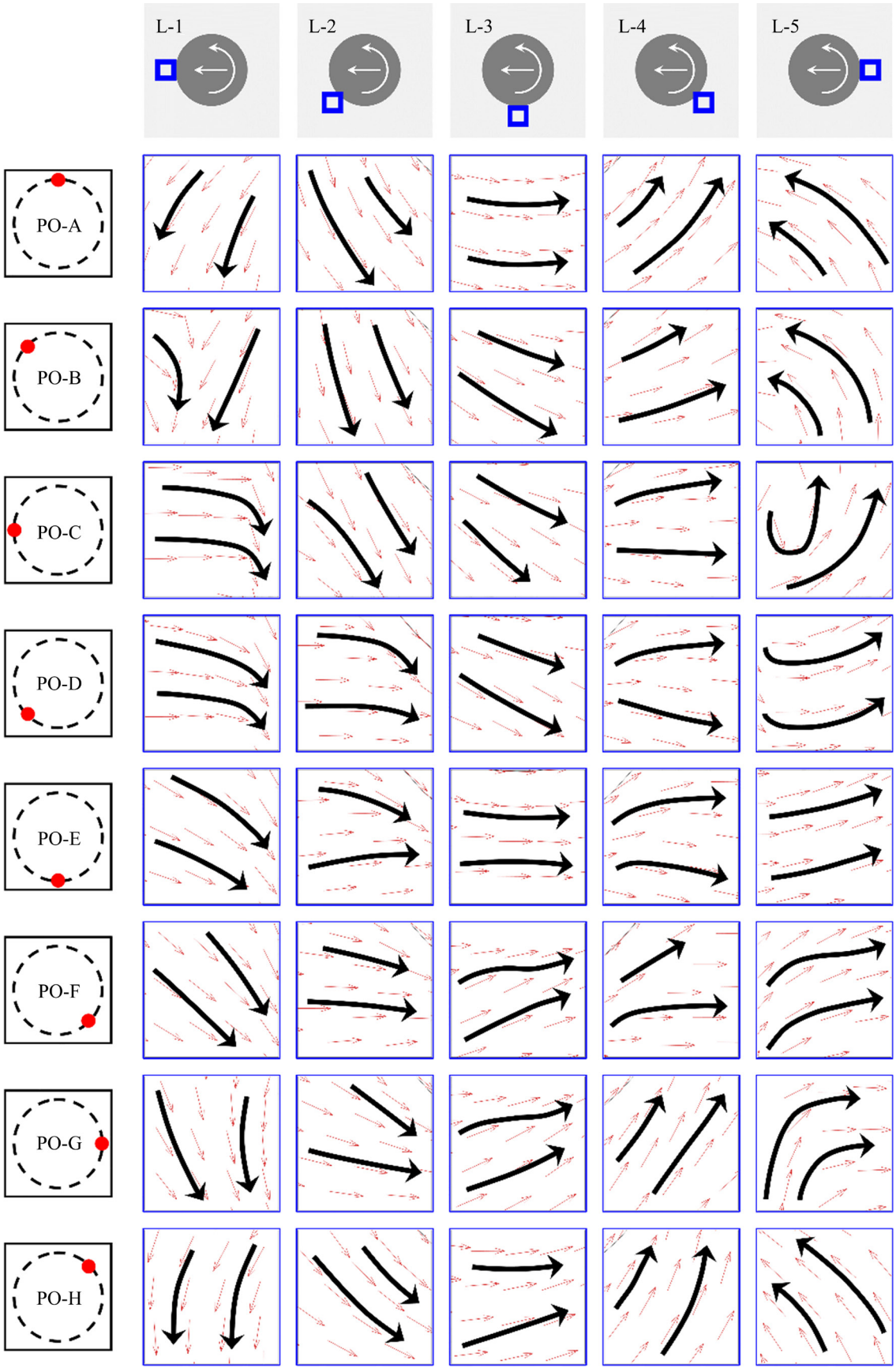

Fig. 13 Evolution of material flow direction around pin at z=−4.5 mm horizontal plane during FSW with tool eccentricity at various pin orientations

feature can be developed and enlarged sequentially since the influence of tool eccentricity on the material flow velocity maintains for a long distance at the back of the pin.

Figures 14 and 15 compare the flow streamlines of the material originally marked at z=−4.5 mm at the front of the tool during FSW without and with tool eccentricity. It is shown that tool eccentricity leads to evident material flow along the vertical direction, as well as disparate material deposition features at various pin orientations at the back of the pin. For welding without tool eccentricity, the material moves upwards increasingly when passing through the pin in both the LE/RS and the TE/RS quadrants, and then moves downwards slightly at the back of the pin. As can be seen, the maximum material moving distance in the vertical direction is less than 0.5 mm, and the material deposition is located mainly at the RS, rather than at the AS.

For welding with tool eccentricity, the evolution of the material flow streamlines are more complex. At PO-A, the material moves upwards quickly for a value ranging broadly from 0 to over

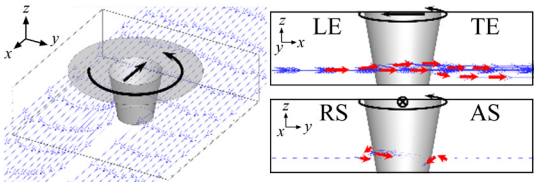

Fig. 14 Flow streamline of material marked at z=−4.5 mm at front of tool during FSW without tool eccentricity

3.0 mm in the LE/AS and the LE/RS quadrants, and then moves downwards gradually in the TE/RS and the TE/AS quadrants. At PO-B, the material continues to move upwards in the TE/RS quadrant for a maximum distance over 3.5 mm, and then moves downwards slightly in the TE/AS quadrant for no more than 2.0 mm. Besides, it is shown that the deposition position of the material is located at both the RS and the AS at the back of the pin, which indicates sufficient material flow and deposition at both PO-A and PO-B. From PO-C to PO-D, the initial position of the upward material flow is postponed from the LE/RS quadrant to the

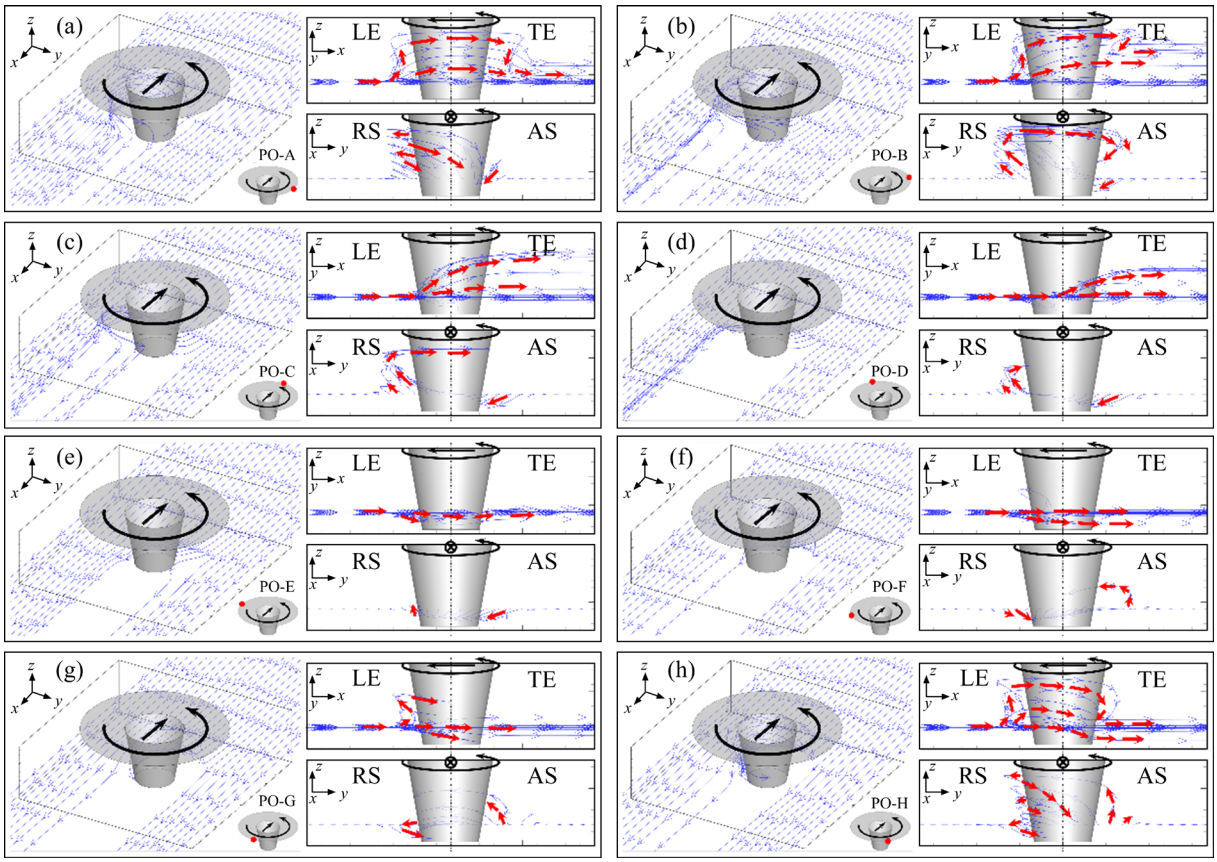

Fig. 15 Flow streamline evolution of material marked at z=−4.5 mm at front of tool during FSW with tool eccentricity at various pin orientations: (a) PO-A; (b) PO-B; (c) PO-C; (d) PO-D; (e) PO-E; (f) PO-F; (g) PO-G; (h) PO-H

TE/RS quadrant with the maximum distance decaying from 3.0 to 2.0 mm, and the downward material flow is indistinctive at both pin orientations. At PO-E, it is shown that only downward material flow exists, and the maximum moving distance is about 1.0 mm. From PO-F to PO-G, the upward material flow emerges again with the maximum moving distance increasing gradually to over 3.0 mm, while the downward material flow maintains relatively stable with the maximum moving distance of less than 1.0 mm. Moreover, another important phenomenon at the pin orientations from PO-C to PO-H is that the material can hardly be deposited in the TE/AS quadrant at the back of the pin, which is opposite to that at PO-A and PO-B. Therefore, it is obvious that tool eccentricity particularly improves the stirring action of the axisymmetric tool during FSW since the material flow along both the horizontal and the vertical directions around the tool is significantly enhanced, which can also be considered as the primary cause for the periodical feature, as well as the onion ring in FSW joint.

4.3 Verification for significance of tool eccentricity

Figure 16 displays the experimental result of the marker material distribution at z=−4.5 mm

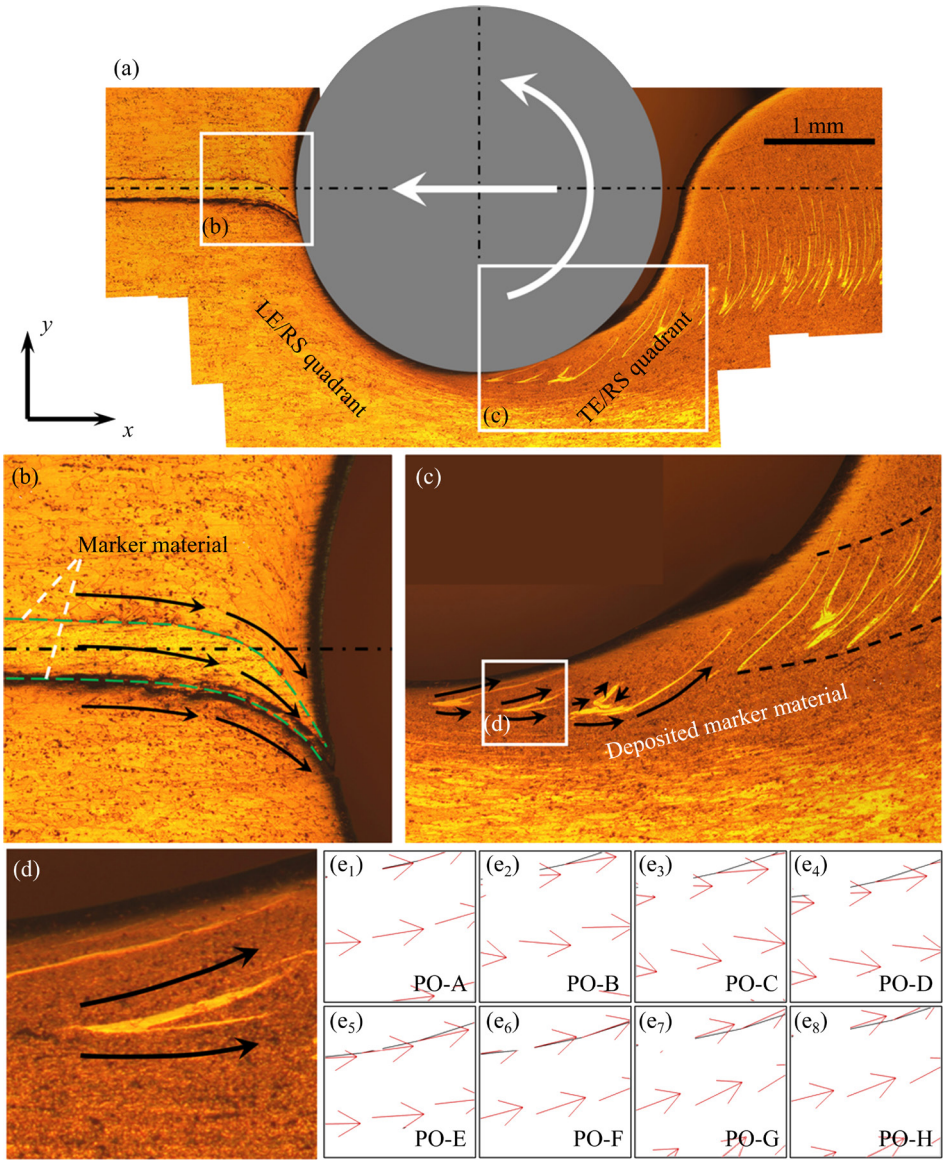

Fig. 16 Illustration of marker material distribution and material flow at z=−4.5 mm horizontal plane around pin: (a) Overall view of marker material distribution; (b) Magnification of marker material at front of pin; (c) Magnification of deposited marker material in TE/RS quadrant; (d) Magnification of periodically deposited marker material; (e_1−e_8) Evolution of material flow direction at pin orientations from PO-A to PO-H in corresponding area of (d) during FSW with tool eccentricity

horizontal plane around the pin, and also demonstrates the comparison of the material flow between experimental and numerical results. It can be seen in Figs. 16(a, b) that the flow direction of the marker material is transformed dramatically into the LE/RS quadrant at the front of the pin, which is consistent with the calculated results of FSW both with and without tool eccentricity. Since the flow velocity magnitude and gradient are both increased, the marker material is strongly elongated and squeezed next to the pin, which can lead to the severe adhesion of the marker material with the tool when the tool is retreated from the workpiece. As a result, the marker material is hardly observed in the LE/RS quadrant. Then, the material starts to be gradually deposited in the TE/RS quadrant and the periodic feature emerges simultaneously, as shown in Fig. 16(c). In this region, it can be seen that the V-shaped periodic deposition feature of the marker material becomes more and more distinct with the decrease of the material velocity, and the feature finally transforms to arc-shaped at the back of the pin. Figure 16(d) magnifies the deposited marker material in the TE/RS quadrant during the formation of the periodic feature, and Figs. 16(e_1−e_8) exhibit the dynamic evolution of the material flow direction at the pin orientations from PO-A to PO-H with tool eccentricity in the corresponding area. The calculated result indicates that the material flow is influenced by tool eccentricity, and the ultimate distribution ranging of the flow direction is found to be in good agreement with the measured one. However, this phenomenon about the periodic deposition of the marker material in FSW has never been reported in numerical results without tool eccentricity. Therefore, the comparative analyses in this study verify the significance of tool eccentricity in FSW since that it is demonstrated to be the primary cause for the periodic material flow behavior.

5 Conclusions

(1) Both the frictional and the volumetric heat densities change periodically with the eccentric movement of the rotating tool. However, the fluctuation amplitudes of the heat density variations in one rotating period are limited. As a result, both the total heat generation and the temperature distribution at different pin orientations during FSW are similar with or without tool eccentricity.

(2) The tool eccentricity induces significant variation of the material flow velocity around the rotating tool. It is found that the material velocity magnitudes and directions in both the horizontal and the vertical directions are changed accordingly at various pin orientations with tool eccentricity during FSW.

(3) The material velocity variation at the RS with tool eccentricity is predominant for the original formation of the periodic material flow and deposition behavior in FSW. Both thermal cycles and marker material distributions obtained by experimentation are found to be matched well with the calculated results with tool eccentricity, rather than without tool eccentricity. Therefore, the critical role of tool eccentricity in FSW process is finally demonstrated.

CRediT authorship contribution statement

Hao SU: Conceptualization, Methodology, Software, Writing − Original draft, Writing − Review & editing, Project administration, Funding acquisition; **Ji CHEN:** Data curation, Methodology, Supervision; **Chuan-song WU:** Writing − Review & editing, Supervision.

Declaration of competing interest

The authors declare that they have no known competing financial interests or personal relationships that could have appeared to influence the work reported in this paper.

Acknowledgments

The authors are grateful to the financial support from the National Natural Science Foundation of China (Nos. 52005297, 52035005), and the Key Research and Development Program of Shandong Province, China (No. 2021ZLGX01).

References

[1] ZHANG Y M, YANG Y P, ZHANG W, NA S J. Advanced welding manufacturing: A brief analysis and review of challenges and solutions [J]. Journal of Manufacturing Science and Engineering−Transaction of the ASME, 2020, 142: 110816.

[2] WU F, FLINT T F, FALCH K V, SMITH M C, DRAKOPOULOS M, MIRIHANAGE W. Mapping flow evolution in gas tungsten arc weld pools [J]. International Journal of Heat and Mass Transfer, 2021, 179: 121679.

[3] WANG Q T, WANG X N, CHEN X M, HUAN P C, DONG Q P, ZHANG Q Y, NAGAUMI H. Interactive effects of porosity and microstructure on strength of 6063 aluminum

alloy CMT MIX plus Synchropulse welded joint [J]. Transactions of Nonferrous Metals Society of China, 2022, 32: 801−811.

[4] MENG X C, HUANG Y X, CAO J, SHEN J J, DOS SANTOS J F. Recent progress on control strategies for inherent issues in friction stir welding [J]. Progress in Materials Science, 2021, 115: 100706.

[5] CHEN S J, LIU J B, JIANG F, XU B, ZHANG G K, LI B. Gravity effects on temperature distribution and material flow in the keyhole pool of VPPA Al welding [J]. International Journal of Heat and Mass Transfer, 2022, 191: 122823.

[6] PADHY G K, WU C S, GAO S. Friction stir based welding and processing technologies−Processes, parameters, microstructures and applications: A review [J]. Journal of Materials Science & Technology, 2018, 34: 1−38.

[7] LIU X C, SUN Z. Numerical simulation of vortex-friction stir welding based on internal friction between identical materials [J]. International Journal of Heat and Mass Transfer, 2022, 185: 122418.

[8] MISHRA R S, Ma Z Y. Friction stir welding and processing [J]. Materials Science and Engineering R: Reports, 2005, 50: 1−78.

[9] RAI R, DE A, BHADESHIA H K D K, DEBROY T. Review: Friction stir welding tools [J]. Science and Technology of Welding and Joining, 2011, 16: 325−342.

[10] VICTOR CHRISTY J, ISMAIL MOURAD A H, SHERIF M M, SHIVAMURTHY B. Review of recent trends in friction stir welding process of aluminum alloys and aluminum metal matrix composites [J], Transactions of Nonferrous Metals Society of China, 2021, 31: 3281−3309.

[11] KRISHNAN K N. On the formation of onion rings in friction stir welds [J]. Materials Science and Engineering A, 2002, 327: 246−251.

[12] CHEN Z W, PASANG T, QI Y. Shear flow and formation of nugget zone during friction stir welding of aluminium alloy 5083-O [J]. Materials Science and Engineering A, 2008, 474: 312−316.

[13] CUI G R, MA Z Y, LI S X. Periodical plastic flow pattern in friction stir processed Al−Mg alloy [J]. Scripta Materialia. 2008, 58: 1082−1085.

[14] NANDAN R, DEBROY T, BHADESHIA H K D H. Recent advances in friction-stir welding-process, weldment structure and properties [J]. Progress in Materials Science, 2008, 53: 980−1023.

[15] NANDAN R, ROY G G, DEBROY T. Numerical simulation of three-dimensional heat transfer and plastic flow during friction stir welding [J]. Metallurgical and Materials Transactions A, 2006, 37: 1247−1259.

[16] ARORA A, NANDAN R, REYNOLDS A P. DEBROY T. Torque, power requirement and stir zone geometry in friction stir welding through modeling and experiments [J]. Scripta Materialia, 2009, 60: 13−16.

[17] ARORA A, DEBROY T, BHADESHIA H K D H. Back-of-the-envelope calculations in friction stir welding–Velocities, peak temperature, torque, and hardness [J]. Acta Materialia, 2011, 59: 2020−2028.

[18] MEHTA M, CHATTERJEE K, DE A. Monitoring torque and traverse force in friction stir welding from input electrical signatures of driving motors [J]. Science and Technology of Welding and Joining, 2013, 18: 191−197.

[19] CHEN G Q, ZHANG S, ZHU Y C, YANG C L, SHI Q Y. Thermo-mechanical analysis of friction stir welding: A review on recent advances [J]. Acta Metallurgica Sinica (English Letters), 2020, 33: 3−12.

[20] CHEN G Q, SHI Q Y, LI Y J, SUN Y J, DAI Q L, JIA J Y, ZHU Y C, WU J J. Computational fluid dynamics studies on heat generation during friction stir welding of aluminum alloy [J]. Computational Materials Science, 2013, 79: 540−546.

[21] ZHANG S, SHI Q Y, LIU Qu, XIE R S, ZHANG G, CHEN G Q. Effects of tool tilt angle on the in-process heat transfer and mass transfer during friction stir welding [J]. International Journal of Heat and Mass Transfer, 2018, 125: 32−42.

[22] SU H, WU C S, PITTNER A, RETHMEIER M. Thermal energy generation and distribution in friction stir welding of aluminum alloys [J]. Energy, 2014, 77: 720−731.

[23] ZHAI M, WU C S, SU H. Influence of tool tilt angle on heat transfer and material flow in friction stir welding [J]. Journal of Manufacturing Processes, 2020, 59: 98−112.

[24] SU H, WU C S, BACHMANN M, RETHMEIER N. Numerical modeling for the effect of pin profiles on thermal and material flow characteristics in friction stir welding [J]. Materials & Design, 2015, 77: 114−125.

[25] DIALAMI N, CERVERA M, CHIUMENTI M, de SARACIBAR A C. A fast and accurate two-stage strategy to evaluate the effect of the pin tool profile on metal flow, torque and forces in friction stir welding [J]. International Journal of Mechanical Sciences, 2017, 122: 215−227.

[26] CHEN G Q, LI H, WANG G Q, GUO Z Q, ZHANG S, DAI Q L, WANG X B, ZHANG G, SHI Q Y. Effects of pin thread on the in-process material flow behavior during friction stir welding: A computational fluid dynamics study [J]. International Journal of Machine Tools & Manufacture, 2018, 124: 12−21.

[27] HUANG Y X< XIE Y M, MENG X C, LI J C, ZHOU L. Joint formation mechanism of high depth-to-width ratio friction stir welding [J]. Journal of Materials Science & Technology, 2019, 35: 1261−1269.

[28] SUN Z, WU C S. Influence of tool thread pitch on material flow and thermal process in friction stir welding [J]. Journal of Materials Processing Technology, 2020, 275: 116281.

[29] GUO N, WANG M R, MENG Q, ZHOU L, TANG D Y. Effect of tool eccentricity on surface periodic banded structures in friction stir welding [J]. IOP Conference Series−Materials Science and Engineering, 2015, 103: 012020.

[30] LEITAO C, ARRUTI E, ALDANONDO E, RODRIGUES D M. Aluminium-steel lap joining by multipass friction stir welding [J]. Materials & Design, 2016, 106: 153−160.

[31] LIU X C, SUN Y F, MORISADA Y, FUJII H. Dynamics of rotational flow in friction stir welding of aluminium alloys [J]. Journal of Materials Processing Technology, 2018, 252: 643−651.

[32] LIU X C, SUN Y F, NAGIRA T, USHIODA K, FUJII H. Experimental evaluation of strain and strain rate during rapid cooling friction stir welding of pure copper [J]. Science and Technology of Welding and Joining, 2019, 24: 352−359.

[33] YAN J H, SUTTON M A, REYNOLDS A P. Processing and

banding in AA2524 and AA2024 friction stir welding [J]. Science and Technology of Welding and Joining, 2007, 12: 390−401.
[34] GRATECAP F, GIRARD M, MARYA S, RACINEUX G. Exploring material flow in friction stir welding: Tool eccentricity and formation of banded structures [J]. International Journal of Material Forming, 2012, 5: 99−107.
[35] FONDA R, REYNOLDS A, FENG C R, KNIPLING K, ROWENHORST D. Material flow in friction stir welds [J]. Metallurgical and Materials Transactions A, 2013, 44: 337−344.
[36] SU H, WANG T, WU C S. Formation of the periodic material flow behavior in friction stir welding [J]. Science and Technology of Welding and Joining, 2021, 26: 286−293.
[37] SU H, CHEN J, WU C S. Effect of tool eccentricity on the periodic material flow in friction stir welding process [J]. International Journal of Mechanical Sciences, 2022, 220: 107164.
[38] SHEPPARD T, JACKSON A. Constitutive equations for use in prediction of flow stress during extrusion of aluminium alloys [J]. Materials Science and Technology, 1997, 13: 203−209.

搅拌头摆动对搅拌摩擦焊接耦合热流行为影响的三维数值模拟

宿 浩，陈 姬，武传松

山东大学 焊接研究所 材料液固结构演变与加工教育部重点实验室，济南 250061

摘 要：提出一种新的三维数值模型，研究搅拌头摆动对搅拌摩擦焊接过程中热流耦合特征的影响。模型中考虑搅拌头在旋转过程中的偏心现象，采用搅拌头−工件界面的非对称边界条件，并使用动态网格技术。研究发现，搅拌头偏心会引起搅拌头−工件界面和剪切层内部热流密度的周期性变化，但是，热流密度变化的波动幅度有限。模拟结果证明搅拌头偏心会使得搅拌头旋转周期内的材料流动行为发生显著变化。此外，材料在后退侧的速度变化对搅拌摩擦焊接周期性特征的形成尤为重要。模拟结果与实验结果吻合良好。

关键词：搅拌摩擦焊接；搅拌头摆动；热行为；周期性材料流动；数值模拟

(Edited by Bing YANG)